

# Deformation of Coal Induced by Methane Adsorption at Geological Conditions

Kan Yang,<sup>†,‡</sup> Xiancai Lu,<sup>\*,†</sup> Yangzheng Lin,<sup>‡</sup> and Alexander V. Neimark<sup>\*,‡</sup>

<sup>†</sup>State Key Lab for Mineral Deposit Research, School of Earth Sciences and Engineering, Nanjing University, 22 Hankou Road, Nanjing 210093, People's Republic of China, and <sup>‡</sup>Chemical and Biochemical Engineering, Rutgers University, 98 Brett Road, Piscataway, New Jersey 08854, United States

Received June 18, 2010. Revised Manuscript Received September 25, 2010

The quenched solid density functional theory (QSDFT) is employed to study methane adsorption on coal at geological conditions. The main focus is made on coal deformation in the course of adsorption that may result in either expansion/swelling or contraction, depending upon the pressure, temperature, and pore size. Two qualitatively different types of deformation behavior were found depending upon the pore width. Type I shows a monotonic expansion in the whole pressure range. This behavior is characteristic for the smallest pores  $< 1.3\sigma_{ff}$  (0.5 nm) that cannot accommodate more than one layer of methane. Type II displays contraction at low pressures followed by expansion. Type II behavior was found for several groups of pores, which can accommodate dense packing with an integer number (from 2 to 6) of adsorbed layers. The results of the QSDFT model are compared to literature experimental data, and the model is employed to study the adsorption behavior of model coals at elevated pressures and temperatures. We established the relationships between the methane capacity and the solvation pressure that it exerts on the coal matrix and the depth of coal bed for pores of different sizes. We found that the coal deformation depends upon the bed depth, and at different depths, it either swells or contracts depending upon the pore size distribution. The implications of these findings for evaluating coal gas resources and coal mine recovery are discussed.

## 1. Introduction

Adsorption of methane on coal plays a crucial role in a variety of natural and technological processes, such as gas outbursts in coal mines,<sup>1,2</sup> global warming caused by methane emissions,<sup>3</sup> evaluation and exploitation of coal methane resources,<sup>4</sup> and methane storage.<sup>5</sup> Natural gas, mainly consisted of methane, is retained in coal beds in three main forms: (1) free gas in cleats, fractures, and macropores, (2) gas dissolved in water formations, and (3) gas adsorbed in micropores of width  $< 2$  nm and mesopores of width from 2 to 50 nm. Adsorption in pores is the primary mechanism of methane retention in coal.<sup>6–8</sup> In the past few years, methane adsorption and adsorption-induced coal swelling and contraction were extensively

investigated depending upon various factors, including pressure, temperature, pore structure, surface properties, coal types, coal ranks, moisture content, mineral matter (ash content), and others.<sup>9–22</sup>

Various empirical methods<sup>10,14–17</sup> as well as the non-local density functional theory (NLDFT)<sup>23</sup> and Grand Canonical Monte Carlo (GCMC) simulation<sup>24</sup> were employed to model methane adsorption capacity. In general, methane adsorption capacity increases with increasing pressure until a certain saturation pressure is reached but decreases with increasing temperature.<sup>9</sup> The effect of the temperature on the storage

\*To whom correspondence should be addressed. Telephone: +86-25-83594664. Fax: +86-25-83686016. E-mail: xcljun@nju.edu.cn (X.L.); Telephone: 1-732-445-0834. E-mail: aneimark@rutgers.edu (A.V.N.).

(1) Bibler, C. J.; Marshall, J. S.; Pilcher, R. C. Status of worldwide coal mine methane emissions and use. *Int. J. Coal Geol.* **1998**, *35*, 283–310.

(2) Díaz Aguado, M. B.; González Nicieza, C. Control and prevention of gas outbursts in coal mines, Riosa–Olloniego coalfield, Spain. *Int. J. Coal Geol.* **2007**, *69*, 253–266.

(3) Banerjee, B.; Dhar, B. Issues and options for reducing methane emission to the atmosphere from Indian coal mining. *Energy Convers. Manage.* **1997**, *37*, 1175–1179.

(4) Gürdal, G.; Yalçın, M. N. Gas adsorption capacity of carboniferous coals in the Zonguldak basin (NW Turkey) and its controlling factors. *Fuel* **2000**, *79*, 1913–1924.

(5) Cui, Y.; Li, Y.; Zhang, Q.; Jiang, W. The characteristic curve of methane adsorbed on coal and its role in the coalbed methane storage research. *Chin. Sci. Bull.* **2005**, *50*, 86–92.

(6) Clarkson, C. R.; Bustin, R. M. Variation in micropore capacity and size distribution with composition in bituminous coal of the Western Canadian Sedimentary Basin. *Fuel* **1996**, *75*, 1483–1498.

(7) Bustin, R. M.; Clarkson, C. R. Geological controls on coalbed methane reservoir capacity and gas content. *Int. J. Coal Geol.* **1998**, *38*, 3–26.

(8) Prinz, D.; Little, R. Development of the micro- and ultramicroporous structure of coals with rank as deduced from the accessibility to water. *Fuel* **2005**, *84*, 1645–1652.

(9) Hildenbrand, A.; Krooss, B. M.; Busch, A.; Gaschnitz, R. Evolution of methane sorption capacity of coal seams as a function of burial history—A case study from the Campine Basin, NE Belgium. *Int. J. Coal Geol.* **2006**, *66*, 179–203.

(10) Levy, J. H.; Day, S. J.; Killingley, J. S. Methane capacities of Bowen Basin coals related to coal properties. *Fuel* **1997**, *76*, 813–819.

(11) Crosdale, P. J.; Moore, T. A.; Mares, T. E. Influence of moisture content and temperature on methane adsorption isotherm analysis for coals from a low-rank, biogenically sourced gas reservoir. *Int. J. Coal Geol.* **2008**, *76*, 166–174.

(12) Bastos-Neto, M.; Canabrava, D. V.; Torres, A. E. B.; Rodriguez-Castellón, E.; Jiménez-López, A.; Azevedo, D. C. S.; Cavalcante, C. L., Jr. Effects of textural and surface characteristics of microporous activated carbons on the methane adsorption capacity at high pressures. *Appl. Surf. Sci.* **2007**, *253*, 5721–5725.

(13) Radovic, L. R.; Menon, V. C.; Leon, C. A. L. Y.; Kyotani, T.; Danner, R. P.; Anderson, S.; Hatcher, P. G. On the porous structure of coals: Evidence for an interconnected but constricted micropore system and implications for coalbed methane recovery. *Adsorption* **1997**, *3*, 221–232.

(14) Crosdale, P. J.; Beamish, B. B.; Valix, M. Coalbed methane sorption related to coal composition. *Int. J. Coal Geol.* **1998**, *35*, 147–158.

(15) Clarkson, C. R.; Bustin, R. M. The effect of pore structure and gas pressure upon the transport properties of coal: A laboratory and modeling study. 1. Isotherms and pore volume distributions. *Fuel* **1999**, *78*, 1333–1344.

(16) Laxminarayana, C.; Crosdale, P. J. Role of coal type and rank on methane sorption characteristics of Bowen Basin, Australia coals. *Int. J. Coal Geol.* **1999**, *40*, 309–325.

capacity of coal is negligible in the range from 25 to 60 °C.<sup>11</sup> A linear decrease of the adsorption capacity with the temperature was reported by Levy et al., with a gradient of approximately  $-0.12 \text{ mL g}^{-1} \text{ K}^{-1}$ .<sup>10</sup> It has been found that samples with higher specific surface area (SSA), higher micropore volume (MPV), and narrower pore size distribution (PSD) have higher methane adsorption capacity.<sup>12</sup> For example, vitrinite-rich coals display a larger MPV and, hence, greater adsorption capacities than inertinite-rich counterparts of the same rank.<sup>13,14,25</sup> Although the ash content imparts a negative effect on the overall adsorption capacity, it can be neglected in the case of micropore adsorption.<sup>16,17</sup> Samples with slightly more hydrophobic surfaces exhibit superior methane adsorption properties compared to less hydrophobic ones.<sup>12</sup> Kurniawan et al.<sup>24</sup> adopted NLDFT and GCMC simulation to study binary adsorption of methane and carbon dioxide in slit-shaped pores, ranging from around 0.75 to 7.5 nm in width. With increasing pressure, the selectivity of carbon dioxide relative to methane in a binary mixture initially increases to a maximum value of  $\sim 35$  bar and, subsequently, drops before attaining a constant value at pressures higher than 300 bar.

While the adsorption capacity was studied in great detail, the adsorption-induced deformation of coal, which can result in gas outburst, still remains an enigmatic problem. Thus far, experimental studies on coal deformation were performed mostly at room temperature and pressures up to 10 MPa, with only a few up to 80 MPa.<sup>26–28</sup> Within these regimes, Levine<sup>26</sup> found a linear swelling ratio of 0.18% in CH<sub>4</sub> at 5.2 MPa. Chikatamarla et al.<sup>29</sup> studied CH<sub>4</sub>-induced swelling on four coal samples with pressures up to 5.0 MPa. The volumetric

strain at 0.6 MPa is found to be from 0.09 to 0.30% for CH<sub>4</sub>. Cui et al.<sup>30</sup> studied the adsorption-induced swelling of three western Canadian coals. The volumetric strain magnitude in their work is up to 0.75%. Sizov et al.<sup>31</sup> studied the influence of pore width, temperature, pressure, and surface properties on the solvation pressure using Monte Carlo and molecular dynamic methods. They adopted either strong (strong adsorption site) or zero (vacancy) local field to account for the surface heterogeneity and found that the effect of vacancies is even more significant than that of strong adsorption sites within the pore width range of 0.65–2.40 nm. Ustinov and Do<sup>22</sup> studied deformation of slit pores adsorbed with subcritical fluid based on NLDFT. Ravikovich and Neimark<sup>20</sup> used the QSDFT model to describe the non-monotonic adsorption-induced deformations typical for microporous zeolites and carbons. They explained this behavior by competition between the attraction of adsorbed molecules to pore walls and packing effects. Pan and Connell<sup>32</sup> developed another theoretical model, which is able to describe the differences in swelling behavior with respect to different gas species and at very high gas pressures, at which the coal swelling reaches a maximum and then decreases. Do et al.<sup>33</sup> used GCMC simulation to study argon adsorption into graphitic slit pores that can deform in the presence of adsorbate by introducing a number of graphic layers at the internal pore surfaces that can move in a direction normal to the surface under the constraint of van der Waals forces. They found that pore widths that are incommensurate with respect to an exact number of layers showed the greatest deformation, especially at high pressure and at higher temperatures. Expansions of up to a 6% increase in the original width for a high adsorbate density were found for the 8 Å pore. Kowalczyk et al.<sup>21</sup> calculated the solvation pressure of argon adsorption on carbide-derived activated carbon at 243 K and up to 1.2 MPa by means of MC simulations and found that the elastic deformation strongly depends upon the PSD. In microporous materials, the reported magnitude of the adsorption-induced elastic moduli may be on the order of gigapascals, which in turn implies very high internal stresses on the order of megapascals.<sup>34,35</sup> Such high stresses can change the stability of coal formations and mining safety during methane recovery and lead to an outburst hazard.<sup>36,37</sup> Although the relationships between solvation pressure and adsorption deformation are well-documented,<sup>20,21</sup> a systematic study of the effect of PSD on coal deformation under supercritical conditions is still lacking.

In this paper, the quenched solid density functional theory (QSDFT) is employed to study methane adsorption

- (17) Faiz, M.; Saghafi, A.; Sherwood, N.; Wang, I. The influence of petrological properties and burial history on coal seam methane reservoir characterisation, Sydney Basin, Australia. *Int. J. Coal Geol.* **2007**, *70*, 193–208.
- (18) Scherer, G. W. Dilatation of porous glass. *J. Am. Ceram. Soc.* **1986**, *69* (6), 473–480.
- (19) Jakubov, T. S.; Mainwaring, D. E. Adsorption-induced dimensional changes of solids. *Phys. Chem. Chem. Phys.* **2002**, *4*, 5678–5682.
- (20) Ravikovich, P. I.; Neimark, A. V. Density functional theory model of adsorption deformation. *Langmuir* **2006**, *22*, 10864–10868.
- (21) Kowalczyk, P.; Ciach, A.; Neimark, A. V. Adsorption-induced deformation of microporous carbons: Pore size distribution effect. *Langmuir* **2008**, *24*, 6603–6608.
- (22) Ustinov, E. A.; Do, D. D. Effect of adsorption deformation on thermodynamic characteristics of a fluid in slit pores at sub-critical conditions. *Carbon* **2006**, *44*, 2652–2663.
- (23) Ravikovich, P. I.; Vishnyakov, A.; Neimark, A. V. Density functional theories and molecular simulations of adsorption and phase transitions in nanopores. *Phys. Rev. E: Stat., Nonlinear, Soft Matter Phys.* **2001**, *64*, 011602.
- (24) Kurniawan, Y.; Bhatia, S. K.; Rudolph, V. Simulation of binary mixture adsorption of methane and CO<sub>2</sub> at supercritical conditions in carbons. *AICHE J.* **2006**, *52*, 957–967.
- (25) Clarkson, C. R.; Bustin, R. M. The effect of pore structure and gas pressure upon the transport properties of coal: A laboratory and modeling study. 1. Isotherms and pore volume distributions. *Fuel* **1999**, *78*, 1333–1344.
- (26) Levine, J. R. Model study of the influence of matrix shrinkage on absolute permeability of coal bed reservoirs. *J. Geol. Soc. (London, U. K.)* **1996**, *109*, 197–212.
- (27) St. George, J. D.; Barakat, M. A. The change in effective stress associated with shrinkage from gas desorption in coal. *Int. J. Coal Geol.* **2001**, *45*, 105–113.
- (28) Cui, X.; Bustin, R. M. Volumetric strain associated with methane desorption and its impact on coalbed gas production from deep coal seams. *AAPG Bull.* **2005**, *89*, 1181–1202.
- (29) Chikatamarla, L.; Cui, X.; Bustin, R. M. Implications of volumetric swelling/shrinkage of coal in sequestration of acid gases. *Proceedings of the 2004 International Coalbed Methane Symposium*; Tuscaloosa, AL, 2004; Paper 0435.
- (30) Cui, X.; Bustin, R. M.; Chikatamarla, L. Adsorption-induced coal swelling and stress: Implications for methane production and acid gas sequestration into coal seams. *J. Geophys. Res.* **2007**, *112*, No. B10202.

---

(31) Sizov, V. V.; Piotrovskaya, E. M.; Brodskaya, E. N. Influence of a surface microheterogeneity on the disjoining pressure of adsorbed Lennard–Jones fluid. Computer simulation. *Colloid J.* **2003**, *65* (6), 772–777.

(32) Pan, Z.; Connell, L. D. A theoretical model for gas adsorption-induced coal swelling. *Int. J. Coal Geol.* **2007**, *69*, 243–252.

(33) Do, D. D.; Nicholson, D.; Do, H. D. Effects of adsorbent deformation on the adsorption of gases in slitlike graphitic pores: A computer simulation study. *J. Phys. Chem. C* **2008**, *112*, 14075–14089.

(34) Balbwna, P. B.; Berry, D.; Gubbins, K. E. Solvation pressures for simple fluids in micropores. *J. Chem. Phys.* **1993**, *97*, 937–943.

(35) Striolo, A.; Chialvo, A. A.; Cummings, P. T.; Gubbins, K. E. Water adsorption in carbon–slit nanopores. *Langmuir* **2003**, *19*, 8583–8591.

(36) White, C. M.; Smith, D. H.; Jones, K. L.; Goodman, A. L.; Jikich, S. A.; LaCount, R. B.; DuBose, S. B.; Ozdemir, E.; Morsi, B. I.; Schroeder, K. T. Sequestration of carbon dioxide in coal with enhanced coalbed methane recovery—A review. *Energy Fuels* **2005**, *19* (3), 659–724.

(37) Colligan, M.; Forster, P. M.; Cheetham, A. K.; Lee, Y.; Vogt, T.; Hriljac, J. A. Synchrotron X-ray powder diffraction and computational investigation of purely siliceous zeolite Y under pressure. *J. Am. Chem. Soc.* **2004**, *126* (38), 12015–12022.

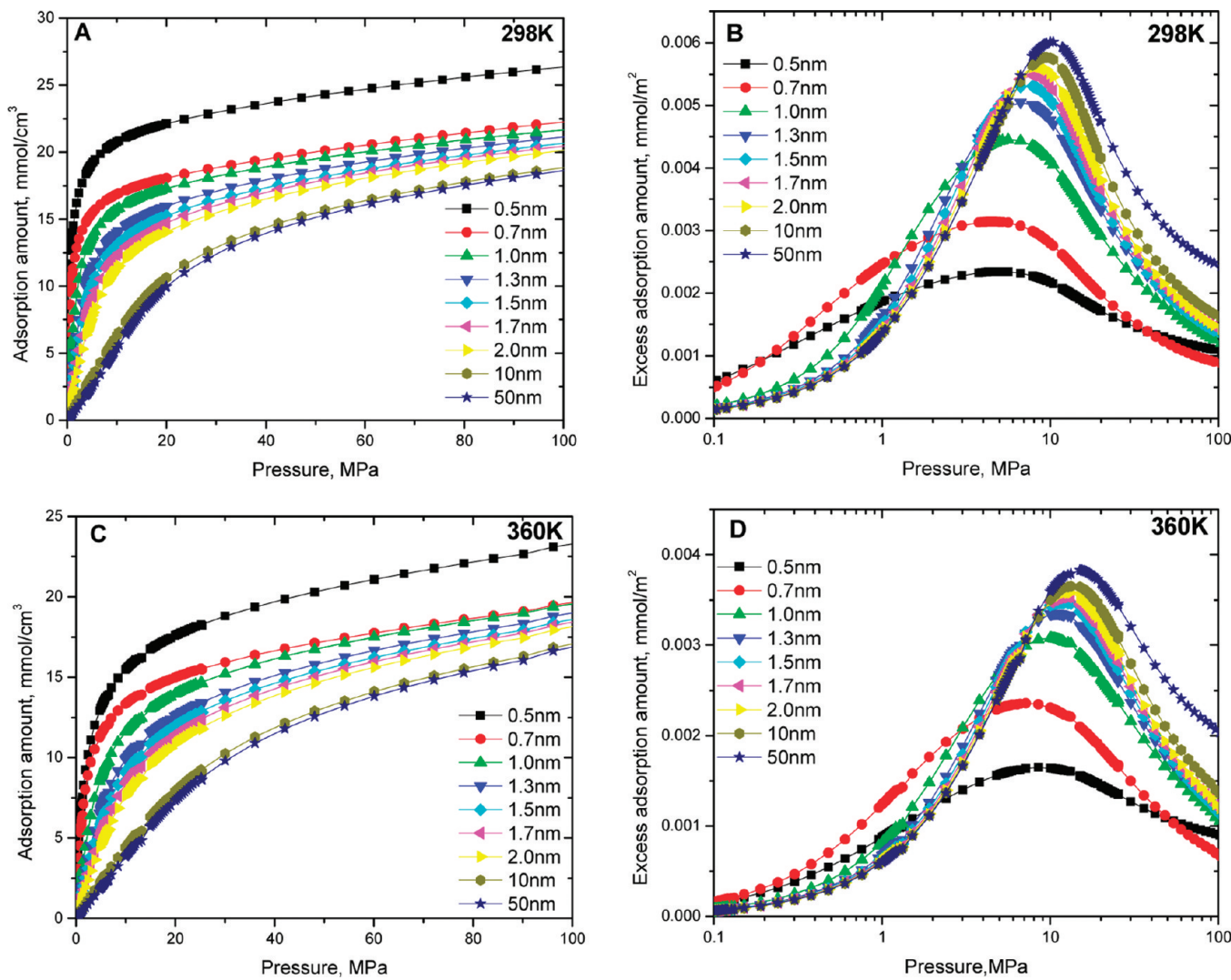


**Figure 1.** Adsorption isotherms of methane in pores of width from 0.5 to 50 nm. (A and B) Isotherms of total adsorption and excess adsorption at 298 K, respectively. (C and D) Isotherms of total adsorption and excess adsorption at 360 K, respectively.

on coal at geological conditions. The main focus is made on coal deformation in the course of adsorption that may result in either expansion/swelling or contraction, depending upon the pressure, temperature, and pore size. In section 2, the QSDFT methodology and the method of calculating adsorption and solvation pressure isotherms are described. The results of methane adsorption capacity, density profile, and salvation pressure on coal in pores from 0.5 to 50 nm at 298 and 360 K with pressure up to 100 MPa are given in section 3. Two qualitatively different types of deformation behavior were found depending upon the pore width. Type I shows a monotonic expansion in the whole pressure range. This behavior is characteristic for the smallest pores  $<1.3\sigma_{ff}$  (0.5 nm) that cannot accommodate more than one layer of methane. Type II displays contraction at low pressures followed by expansion. Type II behavior was found for several groups of pores, which can accommodate dense packing with an integer number (from 2 to 6) of adsorbed layers. Then, the results of the QSDFT model are compared to literature experimental data, and the model is then employed to study the adsorption behavior of model coals at elevated pressures and temperatures. An instructive example of a coal bed with the temperature gradient of 0.03 K/m and the pressure gradient of 0.01 MPa/m is given in section 4. We established the relationships

between the methane capacity and the solvation pressure that it exerts on the coal matrix and the depth of the coal bed for pores of different sizes. We found that the coal deformation depends upon the bed depth, and at different depths, it either swells or contracts depending upon the PSD. In section 5, general conclusions are summarized and the implications of these findings for evaluating coal gas resources and coal mine recovery are discussed.

## 2. Methodology

**2.1. Basic Formulation of QSDFT.** The density functional theory implies that, at the conditions of thermodynamic equilibrium, the spatial distribution of adsorbed species corresponds to a minimum of the grand thermodynamic potential at a given chemical potential, pore volume, and temperature. The QSDFT model is based on the multi-component density functional theory, in which the grand thermodynamic potential  $\Omega$  is defined as

$$\Omega[\{\rho_i(r)\}] = F_{\text{int}}[\{\rho_i(r)\}] + \sum_i \int dr \rho_i(r)[\psi_i(r) - \mu_i] \quad (1)$$

where  $F_{\text{int}}$  is the intrinsic Helmholtz free energy,  $\rho_i$  and  $\mu_i$  are the local number density and chemical potential of component  $i$ , respectively, and  $\psi_i$  is the local external potential.

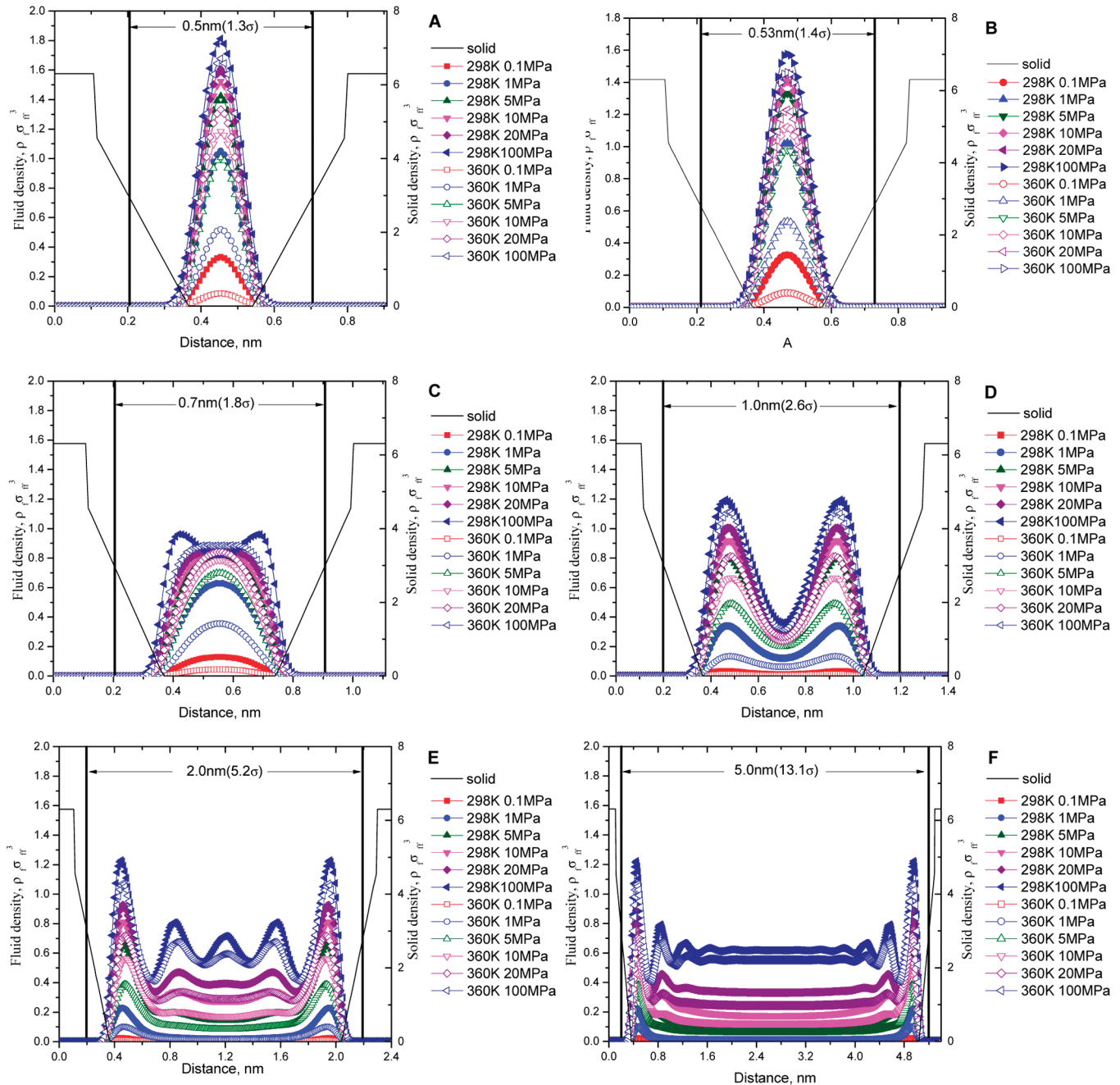


**Figure 2.** Density profile in pores at different pressures and temperatures of 298 and 360 K. The thick solid line represents the pore walls, and the thin line denotes the solid density.

In the QSDFT model of single-component adsorption, we consider the solid as a quenched component of the two-component solid–fluid system. Adsorption interactions are reduced to pairwise interactions between the molecules of adsorbate (fluid) and adsorbent (solid), and external potentials are not considered. Thus, the grand thermodynamic potential is given as

$$\Omega[\rho_s(r); \rho_f(r)] = F_{\text{int}}[\rho_s(r); \rho_f(r)] - \mu_s \int d\mathbf{r} \rho_s(r) - \mu_f \int d\mathbf{r} \rho_f(r) \quad (2)$$

Minimization of the grand thermodynamic potential is performed with respect to the fluid density  $\rho_f(r)$ , keeping the solid density  $\rho_s(r)$  and the contributions from solid–solid atomic interactions unchanged.

$$\delta\Omega[\rho_s(r); \rho_f(r)]/\delta\rho_f(r) = 0 \quad (3)$$

Further detailed information on the QSDFT method is well-documented and can be found in the literature.<sup>38,39</sup>

**2.2. Parameters of Intermolecular Interactions.** The Lennard–Jones (LJ) potential was used to represent both fluid–fluid and fluid–solid interactions. The standard Weeks–Chandler–Andersen (WCA) scheme was adopted to calculate the van der Waals attraction potentials.

$$u_{ij}^{\text{att}}(r) = \begin{cases} -\varepsilon_{ij} & r \leq 2^{1/6}\sigma_{ij} \\ 4\varepsilon_{ij}[(\sigma_{ij}/r)^{12} - (\sigma_{ij}/r)^6] & r \geq 2^{1/6}\sigma_{ij} \end{cases} \quad (4)$$

(38) Ravikovich, P. I.; Neimark, A. V. Density functional theory model of adsorption on amorphous and microporous silica materials. *Langmuir* 2006, 22, 11171–11179.

(39) Neimark, A. V.; Lin, Y.; Ravikovich, P. I.; Thommes, M. Quenched solid density functional theory and pore size analysis of micro–mesoporous carbons. *Carbon* 2009, 47, 1617–1628.

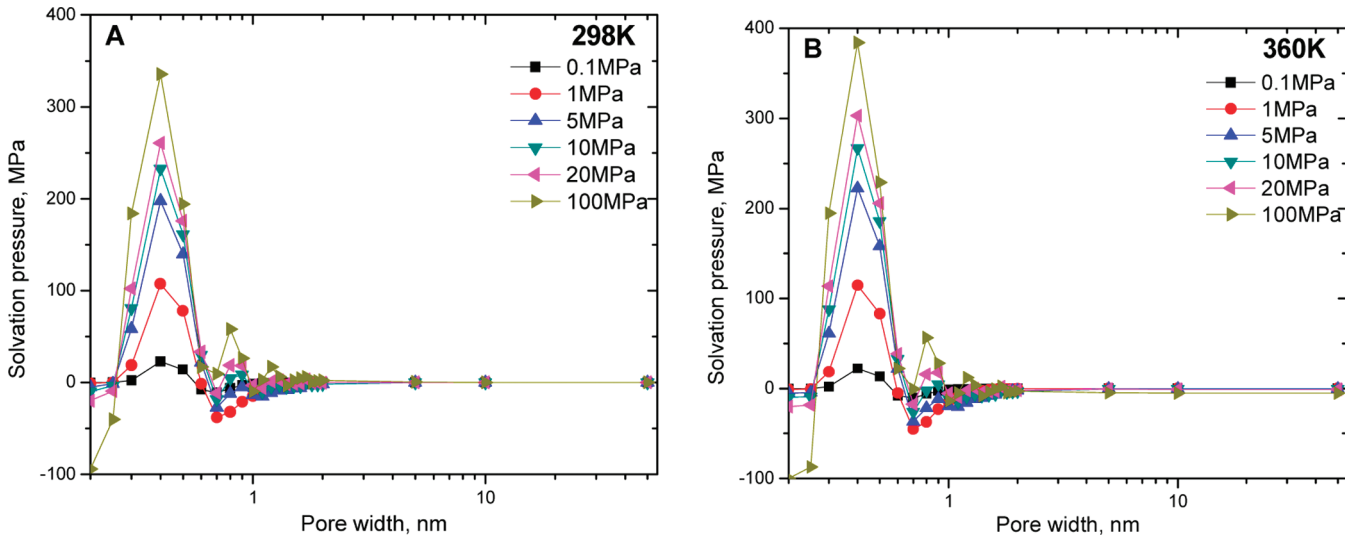


**Figure 3.** Solvation pressure in pores from 0.2 to 50 nm at temperatures of (A) 298 K and (B) 360 K.

For the methane–methane interaction,  $\epsilon_{ff}/k_B = 148.1$  K and  $\sigma_{ff} = d_{HS} = 0.381$  nm. For the carbon–methane interaction, the effective LJ parameters for solid–fluid interactions were chosen as  $\epsilon_{sf}/k_B = 64.4$  K and  $\sigma_{sf} = 0.3605$  nm from combining rules.<sup>40</sup>

**2.3. Porc Model.** Within the QSDFT model, the surface heterogeneity is effectively characterized by the roughness parameter  $\delta$  that represents an average characteristic scale of surface corrugations. We employed the slit pore model developed earlier for nanoporous carbons<sup>39,41</sup> to represent the coal pore geometry. According to the prescription,<sup>39,41</sup> the surface density distribution is described by the following equation:

$$\rho_s(z) = \begin{cases} \rho_s^0 & 0 \leq z < h_0 \\ 0.75\rho_s^0 \left(1 - \frac{z-h_0}{2\delta}\right) & h_0 \leq z < h_0 + 2\delta \\ 0 & z \geq h_0 + 2\delta \end{cases} \quad (5)$$

where  $\rho_s = 0.114 \text{ \AA}^{-3}$  is the density of bulk carbon and  $h_0$  is the effective thickness of the solid wall assumed to be  $h_0 = 2 \times 0.34$  nm. The hard sphere diameter of carbon atoms is 0.2217 nm. The roughness parameter  $\delta$  represents the half-width of the density ramp (5) and was taken as  $\delta = 0.13$  nm.<sup>39</sup>

**2.4. Calculation of Solvation Pressure and Volumetric Strain.** Solvation pressure because of fluid adsorption is the cause of elastic deformation of the adsorbent, which can be measured directly. The calculated solvation pressure may be either positive or negative, which causes either contraction or swelling, respectively.<sup>20–22</sup> The solvation pressure  $f_s$  can be obtained by the following equation:<sup>34</sup>

$$f_s = \frac{1}{A} \left( \frac{\partial \Omega}{\partial H} \right)_{T, \mu, A} - p_\infty \quad (6)$$

where  $A$  is the surface area,  $\Omega$  is the grand free energy,  $H$  is the pore width,  $T$  is the temperature,  $\mu$  is the chemical potential, and  $p_\infty$  is the bulk fluid pressure.

Assuming that the carbon matrix is incompressible, the volumetric strain is given by

$$\varepsilon = \frac{\Delta V}{V} = \frac{\varphi}{k} \bar{f}_s \quad (7)$$

(40) Neimark, A. V.; Ravikovich, P. I. Calibration of pore volume in adsorption experiments and theoretical models. *Langmuir* **1997**, *13*, 5148–5160.

(41) Fitzgerald, J. E.; Sudibandriyo, M.; Pan, Z.; Robinson, R. L., Jr.; Gasem, K. A. M. Modeling the adsorption of pure gases on coals with the SLD model. *Carbon* **2003**, 2203–2216.

where  $\varphi$  is the porosity and  $k$  is the elastic modulus, which is related to the bulk modulus  $K$ , by  $K = k/\varphi$ . Here,  $k$  is assumed to be independent of the pore size.<sup>21</sup>

### 3. Results and Discussion

**3.1. Adsorption Isotherms and Density Profile of Methane in Coal Pores.** The simulated methane adsorption isotherms in porous coal at various pore widths are shown in Figure 1. They belong to the type I adsorption isotherm.<sup>42</sup> The adsorption capacity decreases with increasing temperatures for all pores, as expected.<sup>43–45</sup> As the pressure increases from 0.1 to 10 MPa, the adsorption capacity increases rapidly. When the pressure is higher than 20 MPa, the adsorption capacity increases linearly with the pressure but at a much slower rate. In addition, the adsorption capacity increases with a decreasing pore width (Figure 2). The excess adsorption reaches a maximum at 10–15 MPa. Moffat and Weale found a similar trend in their methane adsorption experiments on 10 coal samples. The apparent adsorption reaches a maximum of 20–61 mL/g [standard temperature and pressure (STP)] at a pressure of 10 or 15 MPa.<sup>46</sup>

From 0.5 to 5 nm, the density profiles in Figure 2 show a typical transition from a one-layer adsorption to that of a multiple-layer adsorption. The density profile at a temperature of 360 K has a similar trend as 298 K, but with a lower density. In the densest case of the 0.5 nm pore, the peak density at 298 K is larger than that of 360 K. This difference in density caused by temperature becomes smaller as the pressure increases. In a 0.7 nm pore, two layers are formed at 100 MPa and 298 K, while at 360 K, only one layer is present. At geological conditions,

(42) Sing, K. S. W.; Everett, D. H.; Haul, R. A. W.; Moscou, L.; Pierotti, R. A.; Rouquerol, J.; Siemieniewska, T. Reporting physisorption data for gas/solid systems with special reference to the determination of surface area and porosity. *Pure Appl. Chem.* **1985**, *57*, 603–619.

(43) Kaneko, K.; Murata, K. An analytical method of micropore filling of a supercritical gas. *Adsorption* **1997**, *3*, 197–208.

(44) Sakurovs, R.; Day, S.; Weir, S.; Duffy, G. Temperature dependence of sorption of gases by coals and charcoals. *Int. J. Coal Geol.* **2008**, *73*, 250–258.

(45) Krooss, B. M.; van Bergen, F.; Gensterblum, Y.; Siemons, N.; Pagnier, H. J. M.; David, P. High-pressure methane and carbon dioxide adsorption on dry and moisture-equilibrated Pennsylvanian coals. *Int. J. Coal Geol.* **2002**, *51*, 69–92.

(46) Moffat, D. H.; Weal, K. E. Sorption by coal of methane at high pressures. *Fuel* **1955**, *34*, 449–462.

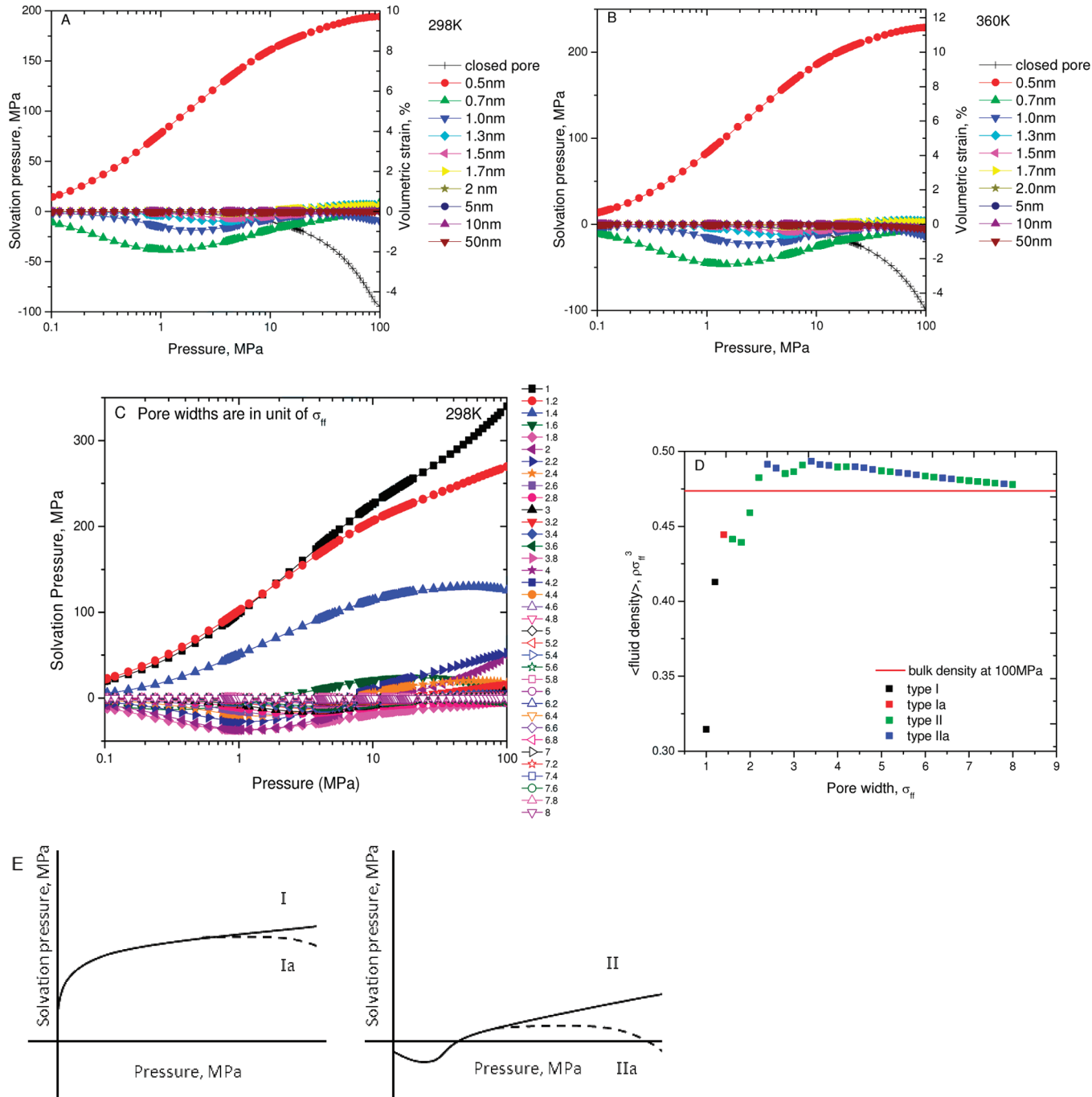


**Figure 4.** Solvation pressure and volumetric strain under external pressures up to 100 MPa. (A and B) Solvation pressure and volumetric strain at 298 and 360 K, respectively. (C) Solvation pressure curve for pores from  $1\sigma_{ff}$  to  $8\sigma_{ff}$  for better understanding of the classification. (D) Average density under different pore widths at 100 MPa. (E) Types of solvation pressure. Detailed classification information for C can be found in the Supporting Information.

in which both pressure and temperature increase with depth, the adsorption capacity may either increase or decrease depending upon the local geothermal gradient.

**3.2. Solvation Pressure and Volumetric Strain.** Figure 3 shows the effect of the pore width on the solvation pressure at temperatures of 298 and 360 K. A non-monotonic dependence of the solvation pressure upon the pore size is found, which is in agreement with findings by Kowalczyk et al.,<sup>21</sup> who studied the deformation of microporous carbon because of supercritical adsorption of argon. From 0.2 nm, the solvation pressure increases quickly to the maximum at ca. 0.4 nm and then decreases to a lower limit around 0.7 nm. For pores larger

than 2 nm, the solvation pressure approaches 0. With increasing temperature, the solvation pressure increases for all pore widths.

The solvation pressure exerted on the walls of micropores is governed by a competition of two major factors: fluid–solid van der Waals attraction that causes pore contraction and hardcore fluid–fluid and fluid–solid repulsion that causes pore expansion because of dense packing of adsorbed molecules. Two qualitatively different types of deformation behavior can be distinguished depending upon the pore size (see Figure 4E). Type I behavior shows a monotonic expansion in the whole pressure range. This behavior is typical for the smallest pores  $< 1.3\sigma_{ff}$  (0.5 nm) that cannot accommodate

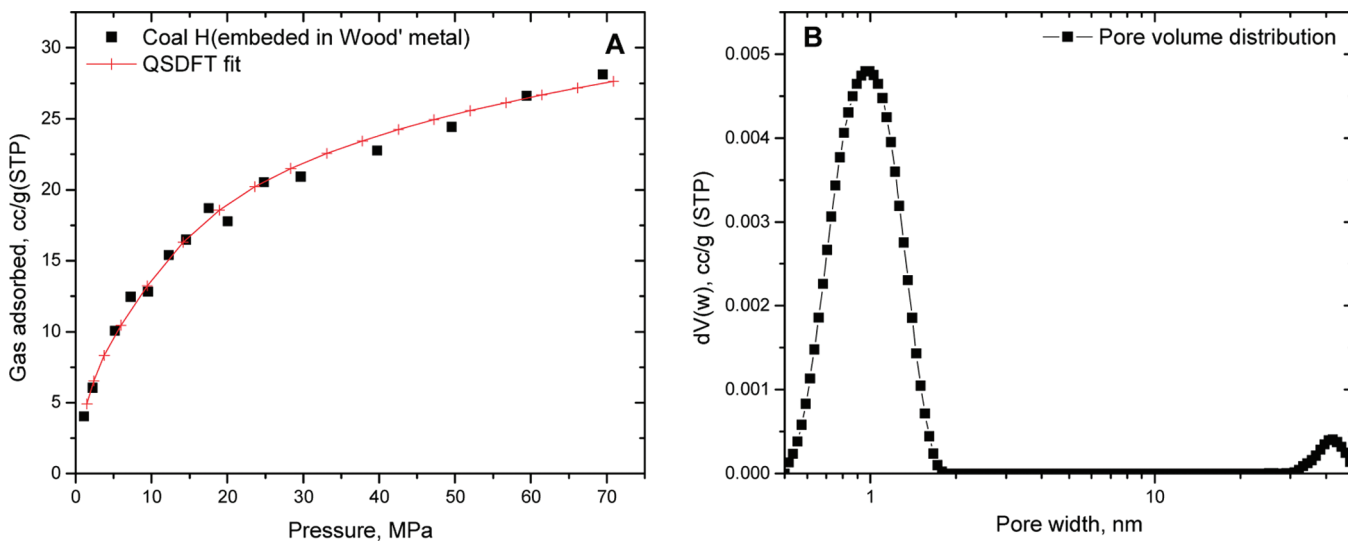


**Figure 5.** (A) Comparison between normalized model methane isotherm and experimental data calculated on the basis of the PSD shown in B. (B) PSD of the sample used in the isotherm calculation.

more than one layer of methane, as shown by the density profile in 0.5 nm pore. In this case, adsorption of additional molecules is necessarily associated with pore expansion. Type II behavior displays contraction at low pressures followed by expansion. This behavior is typical for the pores that can accommodate more than one molecule in their cross-section and is well-documented in the literature for a variety of zeolites and carbons.<sup>47–49</sup> As described in ref 20, the maximum contraction at low pressures caused by attractive adsorbate–solid interactions is achieved at the density of so-called “most comfortable” packing, when the adsorbate molecules are densely packed within a given confinement without overlapping. A further increase of adsorbate density leads to gradual expansion that is required to accommodate additional molecules. This behavior is illustrated by the density profiles in  $1.8\sigma_{ff}$  (0.7 nm) pore (see Figure 2C). The most comfortable packing with one pronounced layer is achieved at  $\sim 1$  MPa that corresponds to the maximum contraction. Type II behavior was found for several groups of pores, which can accommodate dense packings with an integer number (from 2 to 6) of layers (see Figure 4D). However, the solvation pressure magnitude and, respectively, deformation rapidly diminish with the increase of pore sizes. It is worth noting that, because of molecularly rough walls, dense packings are not necessarily regular. In the pores, where the dimensions do not commensurate the dense adsorbate layering, the pore expansion can be followed at sufficiently high pressures by contraction that, in turn, should lead to the packing densification. This effect was observed for both types of deformation behaviors, and the corresponding characteristic strain–pressure curves are given in Figure 4, as Ia and IIa types. Type Ia was found for  $1.4\sigma_{ff}$  pore, with contraction at pressures  $> 57$  MPa. Type IIa behavior was found for several groups of pore sizes, as shown in Figure 4D. Assuming the bulk

(47) Bering, B. P.; Krasilnikova, O. K.; Sarakhov, A. I.; Serpinskii, V. V.; Dubinin, M. M. Alteration of zeolite granule dimensions under krypton adsorption. *Bull. Acad. Sci. USSR, Div. Chem. Sci. (Engl. Transl.)* 1977, 26, 2258–2261.

(48) Krasilnikova, O. K.; Bering, B. P.; Serpinskii, V. V.; Dubinin, M. M. Deformation of zeolite CaNaX during xenon adsorption. *Bull. Acad. Sci. USSR, Div. Chem. Sci. (Engl. Transl.)* 1977, 26, 1099–1101.

(49) Fomkin, A. A. Adsorption of gases, vapors and liquids by microporous adsorbents. *Adsorption* 2005, 11, 425–436.

**Table 1. Parameters Used in the Calculation of Volumetric Strain (298 K)**

	bulk modulus (GPa)	model PSD (%)			
		closed pores	0.5 nm	0.7 nm	50 nm
coal A <sup>46</sup>	2	15 50	2.2 9.5	2 0	80.8 40.5
coal B <sup>46</sup>	2	10 18.5	8 11	10 5	72 65.5
coal C <sup>46</sup>	2	14 42	7.2 18	5 35	73.8 5
coal D <sup>46</sup>	2	18 40	5 13.1	8 20	69 26.9
coal E <sup>46</sup>	2	16	23.5	55	5.5
coal F <sup>46</sup>	2	8	24.5	35	32.5
coal G <sup>26</sup>	2	4	9.6	10.5	75.9
coal H <sup>30</sup>	3	7	5.5	3	84.5

modulus of 2 GPa,<sup>32,50</sup> we found that the volumetric strain in micropores is significant, varying from 10% (0.5 nm) to  $-2\%$  (0.7 nm), which is consistent with other estimates.<sup>32</sup> Note that the deformation in pores  $> 2.1$  nm ( $5.6\sigma_{ff}$ ) is negligibly small,  $< 0.1\%$ .

**3.3. Comparison to Experiments.** *3.3.1. Methane Adsorption Capacity.* The experimental isotherm is taken from the paper of Moffat and Weal,<sup>46</sup> where a cylindrical block of coal H was immersed in molten Wood’s metal. The molten Wood’s metal was solidified, leaving a hole of about 0.125 in. in diameter accessible by methane. This method allows for the isotherm to be measured, preventing coal expansion. The PSD was obtained by the QSDFT method.<sup>39</sup> With this PSD, the calculated isotherm fits the experimental data quite well (Figure 5).

*3.3.2. Volumetric Strain.* We attempted to describe the experimental deformation data of Moffat and Weal,<sup>46</sup> Levine,<sup>26</sup> and Cui et al.<sup>30</sup> by varying the PSDs. The PSD (see Table 1) was determined to give the best fit with the experiment. Because of the lack of PSD information, we use four pores (closed, 0.5 nm, 0.7 nm, and 50 nm pores) in different proportions to account for

(50) Medhurst, T. P. Estimation of the in-situ strength and deformability of coal for engineering design. Ph.D. Thesis, Department of Mining, Minerals, and Materials Engineering, The University of Queensland, Brisbane, Queensland, Australia, 1996.

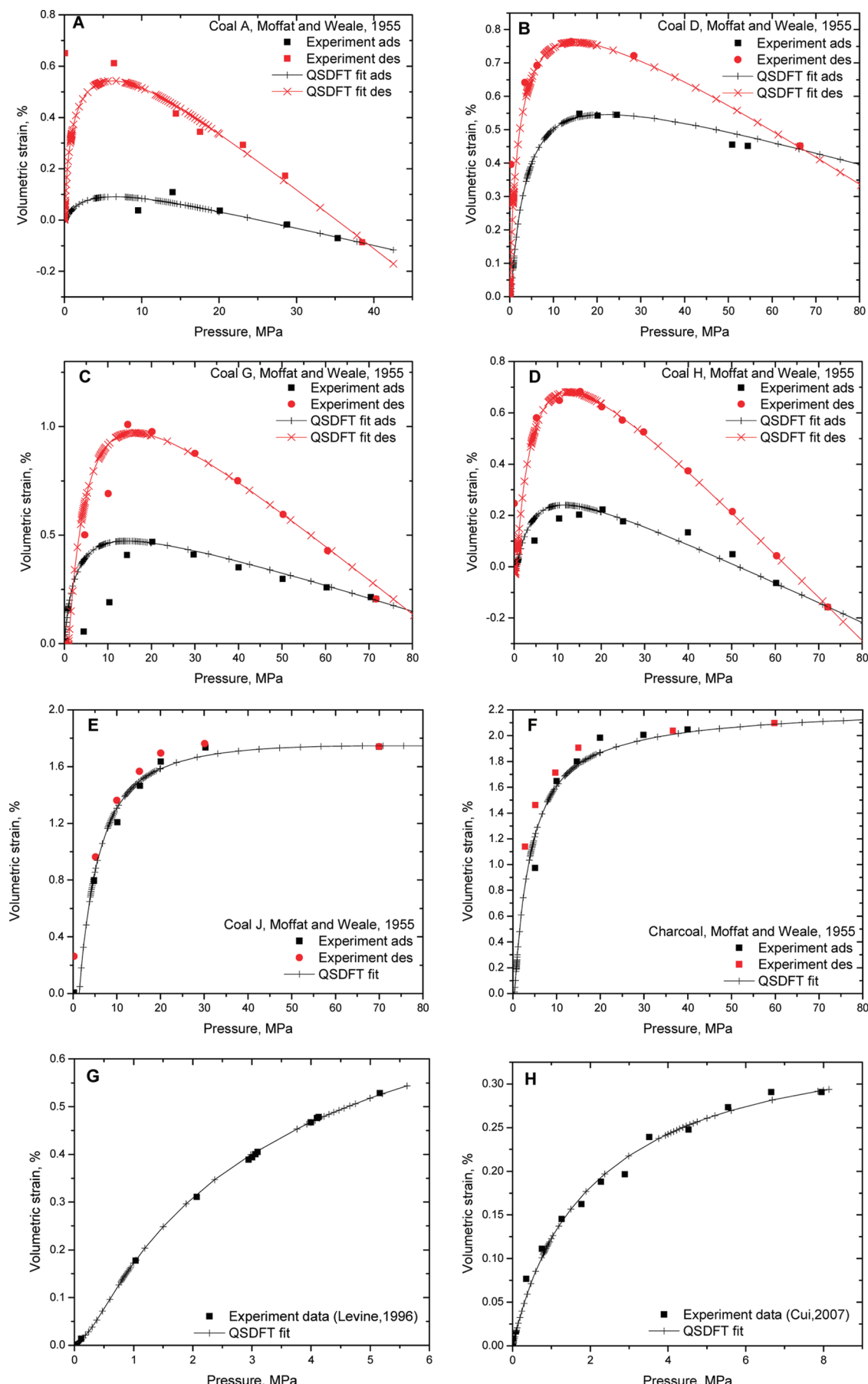


**Figure 6.** Calculated adsorption-induced volumetric strain compared to experimental data: (A–F) data from Moffat and Weal,<sup>46</sup> (G) data from Levine,<sup>26</sup> and (H) data from Cui et al.<sup>30</sup>

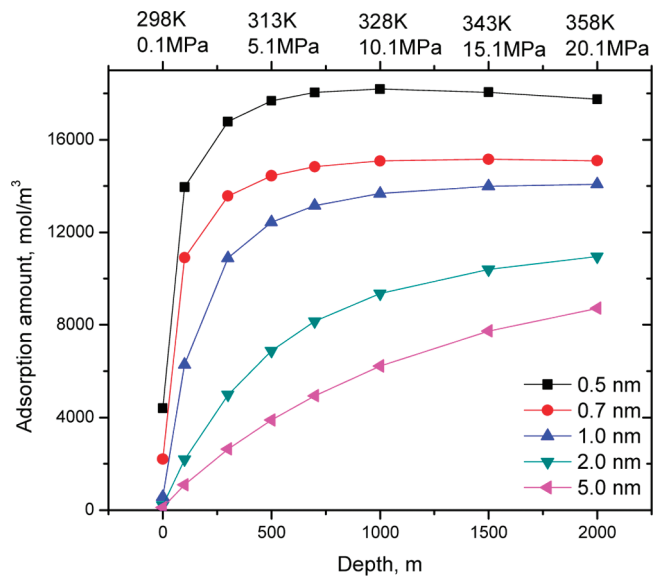


**Figure 7.** Combined effects of the temperature and pressure on the adsorption capacity of coal pores under geological conditions.

the effect of the pore size. The bulk modulus of the samples by Moffat and Weale and Levine was taken as 2 GPa, which is consistent with a general estimate of the bulk modulus of 1–3 GPa for black coal.<sup>51</sup> The bulk modulus of the sample by Cui et al. is taken from ref 30. The results of our theoretical predictions of the volumetric strain in comparison to experiments are given in Figure 6. Because all experimental data available are of type I, the theoretical dependences in Figure 6 were calculated by fitting the experimental data by varying the PSD with restriction to non-negative strains. Note that, for the samples that show a significant hysteresis, the fitted PSDs for adsorption and desorption data are quite distinct, which confirms an irreversible change in the coal pore structure at high pressure sorption.

It is worth noting that Pan and Connell<sup>32</sup> developed an energy balance model to describe adsorption-induced volumetric changes. They used the Langmuir equation to mimic the experimental isotherm. The calculated volumetric strain was consistent with the desorption branch of the coal deformation curves of Moffat and Weale<sup>46</sup> and Levine.<sup>26</sup>

#### 4. Methane Adsorption on a Model Coal

Consider a coal bed model in a basin with a temperature gradient of 0.03 K/m, pressure gradient of 0.01 MPa/m, and bulk modulus of 2 GPa. The variation of the methane density with bed depth in pores of different sizes is given in Figure 7. Obviously, micropores ( $\leq 2$  nm) present much higher adsorption capacity than the mesopores ( $> 2$  nm). The adsorption capacity of pores ( $\leq 1$  nm) increases tremendously with depth and reaches a maximum amount of ca.  $14\,000 \text{ mol/m}^3$  at a depth of about 500 m. In contrast, for 5 nm pore, the adsorption capacity keeps increasing even as the depth reaches 2000 m, indicating that it might have a greater effect on the adsorption capacity at deeper levels ( $> 2000$  m). For the coal mine recovery process, great attention should be paid to the coals possessing large fractions of micropores. It is worth noting that the equilibrium adsorption amount in the pores at the depth of 100 m is about 3–11 times than that on the

(51) Wang, G. X.; Massarotto, P.; Rudolph, V. An improved permeability model of coal for coalbed methane recovery and CO<sub>2</sub> geosequestration. *Int. J. Coal Geol.* 2009, 77, 127–136.

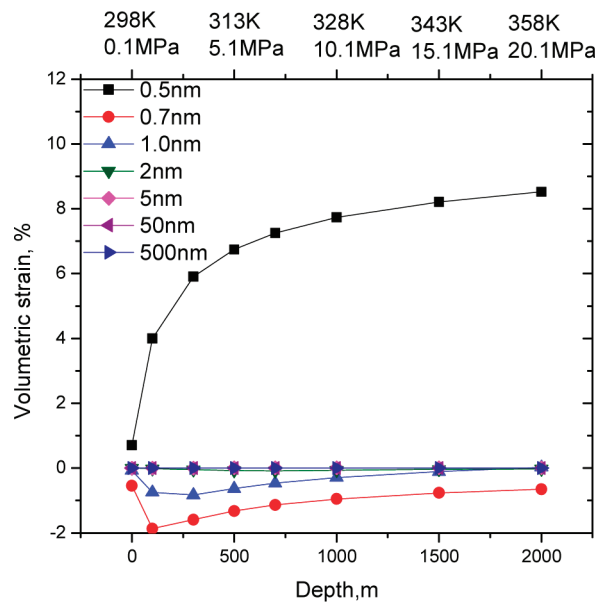


**Figure 8.** Volumetric strain induced by methane adsorption in coal pores with various pore widths.

ground. In this calculation, the greatest amount exerted comes from the pores with a width of 0.5 nm. Our calculations correspond to the general conclusion that micropore volume is the controlling factor for all gas adsorption capacities of coals.<sup>25</sup>

The adsorption-induced deformation behavior is given in Figure 8. Three types of strain-depth dependences are observed. First, in the case of 0.5 nm pore, the volumetric strain increases quickly, with buried depth increasing up to 500 m, and then slowly increases afterward. Second, for pores of 0.7 and 1 nm, volumetric strain decreases to a minimum when the depth is about 100 m and then slowly increases, diminishing as the depth increases. Third, for pores  $\geq 2$  nm, the volumetric strain is negligible at all of the depths. To mimic the condition of coal recovery, with the depth drop up to 1000 m, it is obvious that the solvation pressure in the micropores will have the dominating effect. On one hand, if the coal is comprised mainly of micropores of  $\sim 0.5$  nm width, the coal is expected to swell significantly. On the other hand, larger micropores of 0.7–1.0 nm contribute to the coal contraction. Thus, the pore size distribution should be taken in account as one of the major factors affecting coal deformation. Special attention should be paid to the working depths around 100 m, because the volumetric strain changes with the depth very rapidly, which may lead to a gas outburst with a sudden drop of pressure during unloading.

#### 5. Conclusions

We employed the QSDFT model to study methane adsorption on coal at geological conditions. We established the relationships between the methane capacity and the solvation pressure that it exerts on the coal matrix and the depth of coal bed for pores of different sizes. Our results are compared to literature experimental data, and the model is then employed to study the adsorption behavior of model coals at elevated pressures and temperatures. It provides a useful tool to better understand the adsorption-induced deformation problem, highlighted by the following two points.

(1) Adsorption capacity: The micropore volume is the controlling factor of the coal adsorption capacity. The highest

adsorption capacity per unit pore volume is exhibited by pores of width around 0.5 nm. For larger pores, the adsorption capacity decreases with the pore width. From the excess adsorption isotherms, the adsorption amount increases rapidly with pressure to 10–15 MPa (corresponding to about 1000–1500 m in depth), where it reaches a maximum. For the purpose of resource evaluation of coal gas, the coal formation at depth > 500 m has a greater potential to adsorb more methane in micropores.

(2) Adsorption-induced deformation effect: The coal deformation depends upon the bed depth, and at different depths, it either swells or contracts depending upon the pore size distribution. Two qualitatively different types of deformation behaviors were found depending upon the pore width. Type I shows a monotonic expansion in the whole pressure range. This behavior is characteristic for the smallest pores  $< 1.3\sigma_{ff}$  (0.5 nm) that cannot accommodate more than one layer of methane. Type II displays contraction at low pressures

followed by expansion. Type II behavior was found for several groups of pores, which can accommodate dense packing with an integer number (from 2 to 6) of adsorbed layers. Special attention should be paid to the working depths around 100 m, because the volumetric strain changes with the depth very rapidly, which may lead to a gas outburst with a sudden drop of pressure during unloading.

**Acknowledgment.** We acknowledge the National Science Foundation of China (40673041 and 40973029). This work was supported in part by the National Science Foundation (NSF) Engineering Research Center (ERC) “Structured Organic Particulate Systems” and the Blaise Pascal International Research Chair Fellowship to A.V.N.

**Supporting Information Available:** Detailed classification information in Figure 4C. This material is available free of charge via the Internet at <http://pubs.acs.org>.